energies

MDPI

Article

Analyzing the Impacts of System Parameters on MPC-Based Frequency Control for a Stand-Alone Microgrid

Thai-Thanh Nguyen, Hyeong-Jun Yoo and Hak-Man Kim *

Department of Electrical Engineering, Incheon National University, Songdo-dong, 119 Academy-ro, Yeonsu-gu, Incheon 22012, Korea; ntthanh@inu.ac.kr (T.-T.N.); yoohj@inu.ac.kr (H.-J.Y.)

* Correspondence: hmkim@inu.ac.kr; Tel.: +82-32-835-8769

Academic Editor: Wenxin Liu

Received: 8 February 2017; Accepted: 20 March 2017; Published: 23 March 2017

Abstract: Model predictive control (MPC) has been widely studied for regulating frequency in stand-alone microgrids (MGs), owing to the advantages of MPC such as fast response and robustness against the parameter uncertainties. Understanding the impacts of system parameters on the control performance of MPC could be useful for the designing process of the controller to achieve better performance. This study analyzes the impact of system parameters on the control performance of MPC for frequency regulation in a stand-alone MG. The typical stand-alone MG, which consists of a diesel engine generator, an energy storage system (ESS), a wind turbine generator, and a load, is considered in this study. The diesel engine generator is in charge of primary frequency control whereas the ESS is responsible for secondary frequency control. The stand-alone MG is linearized to obtain the dynamic model that is used for designing MPC-based secondary frequency control. The robustness of MPC against the variation of system parameters is also analyzed in this study. A comparison study of MPC and proportional–integral (PI) control is presented. Simulation results show that MPC has a faster response time and lower overshoot compared to PI control. In addition, the robustness of MPC against the system uncertainties is stronger than conventional PI control.

Keywords: model predictive control; secondary frequency control; system parameter uncertainties; stand-alone microgrid

1. Introduction

A stand-alone microgrid (MG) is a small-scale power system that can operate separately from the utility grid. The inertia time constant of the stand-alone MG system is relatively small due to the lack of synchronization with the utility grid, which results in the difficulty of frequency control [1–3]. The frequency control units should rapidly compensate for the imbalance between the power supplies and power demands to minimize the frequency deviation. Since the penetration of renewable energy resources such as wind generation with the major issues of variability and uncertainty increase, frequency control in a stand-alone MG now faces more challenges [4,5]. The frequency controller should be designed properly to ensure the stability of the MG system.

Diesel-engine generators with a droop speed regulator are responsible for the primary frequency control of the stand-alone MG system, which might cause steady-state frequency deviation from the nominal value. Conventionally, automatic generation control (AGC) has been developed to compensate for the steady-state error that is caused by the primary frequency control. However, the conventional scheme of AGC might be difficult for obtaining a desirable performance due to the low inertia time constant of the MG system and the high penetration of wind generation [6,7]. The energy storage systems (ESSs) with the function of secondary frequency control, which might be a battery

energy storage system (BESS), flywheel energy storage system (FESS), or superconducting magnetic energy storage (SMES), have been used in the stand-alone MG system to improve the performance of frequency regulation [8,9]. Several control techniques have been studied for the secondary frequency control of the stand-alone MG system. A typical proportional-integral (PI) control is considered as the practical implementation for secondary frequency control due to its straightforward characteristic. However, the designed PI parameters might not provide the desirable performance for a wide range of operations. Intelligent frequency control based on an online particle swarm optimization (PSO)-based fuzzy tuning approach has been presented to optimize PI parameters automatically according to online measurements [10,11]. For the stand-alone MG system using these control strategies, it is difficult to effectively obtain the tradeoff between the nominal and robust performances for a wide range of disturbances and uncertainties [12]. Robust frequency control techniques, which consider the uncertainties of the MG system, have been proposed to improve the robustness of the MG system as well as the nominal performance [13–16]. However, requiring a priori known bounds on uncertainties is one of the disadvantages of robust frequency control. Additionally, it is difficult to guarantee the asymptotic stability of the tracking error performance of robust control [17].

Recently, model predictive control (MPC) has been widely studied in MG control. The receding horizon principle of MPC is the key feature that distinguishes MPC from the other control strategies. A finite horizon optimal control problem, which is formulated by a cost function, is solved over the prediction horizon at each sample. The dynamic model of the plant is used to predict the future variables that are used to solve the optimization problem [18]. Several studies have presented the MPC-based frequency control of the stand-alone MG system. MPC-based coordinated frequency control of wind generations and plug-in hybrid electric vehicles (PHEVs) presented in [19] could be used for a MG system in which the penetration of wind generation is relatively high. Multiple MPCs-based frequency regulation, which can switch the controllers according to the change of the operating conditions, has been presented in [20,21]. A compound control strategy, which consists of a MPC-based upper level for generators and a distributed leader-following consensus control strategy at the lower level for multiple energy storage units, has been proposed in [22]. Since the control performance of MPC relies on the MG system parameters, understanding the most sensitive parameters to the MPC could be useful for the designing process to achieve better performance. However, the impacts of MG system parameters on the control performance of MPC have not been studied in previous works. The contribution of this study is to evaluate the impacts of system parameters on MPC-based frequency control of the stand-alone MG system. In addition, a comparison study of MPC and PI control for frequency regulation is presented to show the effectiveness of MPC-based frequency control. The PI parameters are tuned automatically according to [23] to achieve the effective comparison.

The rest of this paper is arranged as follows. Section 2 presents the case study of a stand-alone MG system and the designing process of MPC-based secondary frequency control. The state-space dynamic model of the MG system that is used for designing the controller is developed in this section. Simulation results are presented in Section 3. The frequency responses to the load change and to the fluctuation in wind powers are shown. The control performances of the MPC and PI controllers when the system parameters change are evaluated in this section. Finally, the conclusions are summarized in Section 4.

2. Stand-Alone MG and MPC-Based Secondary Frequency Control

2.1. Stand-Alone MG

Figure 1 shows the configuration of a stand-alone MG that consists of wind turbine generator (WTG), a load, an ESS, and a diesel-engine generator (DG). The frequency deviation is caused by the disturbance between the power demands and power supplies. In addition, the MG frequency is also deviated by the change of wind speed. The DG with primary frequency control should generate

power rapidly to adapt for the changes of power demand or power supply. The primary frequency control is based on the droop speed control strategy, which results in the steady-state error of frequency. To recover the frequency to the nominal value, the secondary frequency control that is based on the MPC strategy is applied to the ESS. The nominal power of each component in the MG adopted from [10], in which the nominal power of WTG, DG, ESS and Load are 100 kVA, 160 kVA, 90 kWh, and 200 kW, respectively.

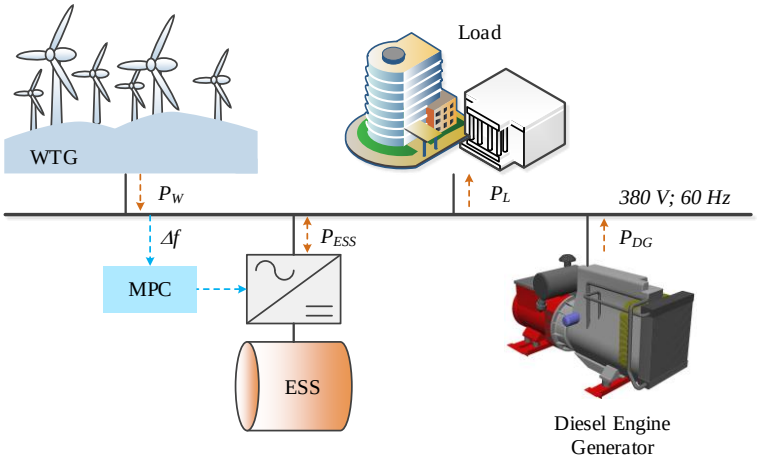

Figure 1. Topology of a stand-alone microgrid.

In order to evaluate the frequency response of the stand-alone MG system, the linearized model of the stand-alone MG, which is widely studied for analyzing the frequency response of the MG system [10,12,24,25], is shown in Figure 2. The dynamic model of DG consists of the turbine model, governor model, and speed control loop. The fixed-speed wind turbine generator based on an induction generator is considered. The dynamic model of such a wind turbine generator is simplified as a first-order transfer function in which the time constant (T_W) is relatively large [12]. Owing to the rapid injection of stored energy, the ESS can be modeled as a first-order transfer function that has a small time constant (T_E) [24]. The DG is in charge of primary frequency control whereas the ESS is responsible for secondary frequency control. The system parameters are given in Table 1.

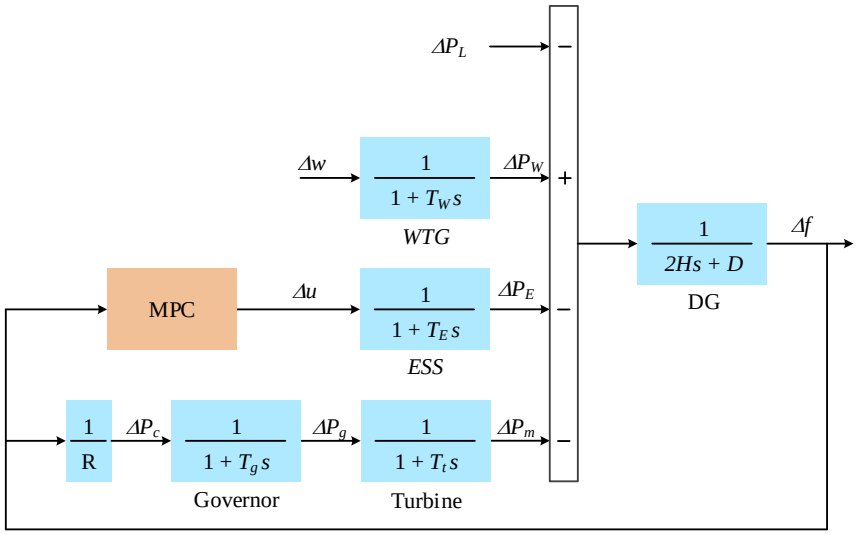

Figure 2. Linearized model of a stand-alone MG.

Table 1. System parameters [10].

Parameter	Value	Parameter	Value
$2H$ (s)	0.1667	R (Hz/pu)	3
D (pu/Hz)	0.015	T_W (s)	1.5
T_g (s)	0.08	T_E (s)	0.1
T_t (s)	0.4	-	-

2.2. Designing MPC-Based Secondary Frequency Control

The state-space dynamic model of the stand-alone MG is shown in Figure 2, which is used for designing the MPC-based secondary frequency control, is given by Equation (1).

$$\begin{aligned} \dot{x} &= Ax + Bu \\ y &= Cx \end{aligned} \tag{1}$$

where:

$$x^T = \begin{bmatrix} \Delta P_E & \Delta P_W & \Delta P_g & \Delta P_m & \Delta f & \Delta w & \Delta P_L \end{bmatrix} \tag{2}$$

$$u = [\Delta u] \tag{3}$$

$$A = \begin{bmatrix} -\frac{1}{T_E} & 0 & 0 & 0 & 0 & 0 & 0 \\ 0 & -\frac{1}{T_W} & 0 & 0 & 0 & \frac{1}{T_W} & 0 \\ 0 & 0 & -\frac{1}{T_g} & 0 & \frac{1}{R.T_g} & 0 & 0 \\ 0 & 0 & \frac{1}{T_t} & -\frac{1}{T_t} & 0 & 0 & 0 \\ -\frac{1}{2H} & \frac{1}{2H} & 0 & -\frac{1}{2H} & -\frac{D}{2H} & 0 & -\frac{1}{2H} \\ 0 & 0 & 0 & 0 & 0 & 0 & 0 \\ 0 & 0 & 0 & 0 & 0 & 0 & 0 \end{bmatrix} \tag{4}$$

$$B^T = \begin{bmatrix} \frac{1}{T_E} & 0 & 0 & 0 & 0 & 0 & 0 \end{bmatrix} \tag{5}$$

$$C^T = \begin{bmatrix} 0 & 0 & 0 & 0 & 1 & 0 & 0 \end{bmatrix} \tag{6}$$

Here, x and u are the state vector and control signal vector, respectively; y is the output vector; Δu is the control increment; A, B, and C are the system matrices.

Two phase operation of the MPC is shown in Figure 3, which consists of the state estimation phase and optimization phase [18]. State estimation can be obtained by measuring the current state variables, in which the future trend of state variables is estimated by using the prediction model, as given by Equation (7).

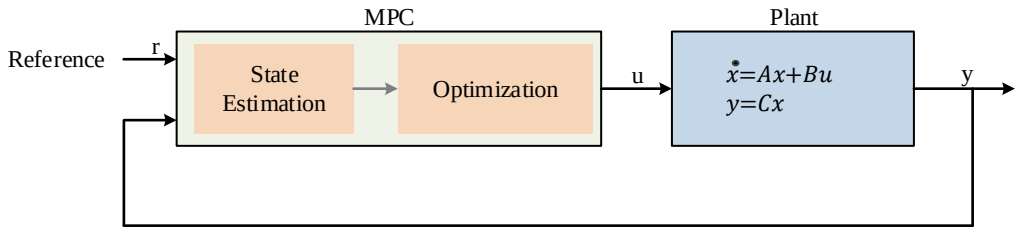

Figure 3. Model predictive control (MPC) operation.

$$\begin{aligned} x(k+1) &= Ax(k) + Bu(k) \\ y(k) &= Cx(k) \end{aligned} \tag{7}$$

The second phase of the controller is to minimize the cost function (Equation (8)) to obtain the control action at time k. The first term of the cost function is the penalizing deviation of the control variable that is the frequency in this paper. The second term of the cost function is used to minimize the variations in the control signals of the ESS.

$$J(k) = \sum_{i=0}^{H_p} \| y(k+i|k) - r(k+i|k) \|_Q^2 + \sum_{i=0}^{H_u-1} \| \Delta u(k+i|k) \|_R^2 \tag{8}$$

where $y(k+i|k)$ is the predicted controlled output at time k; $\Delta u(k+i|k) = u(k+i) - u(k+i-1)$ is the predicted control increment; $r(k+i|k)$ is the reference at time k; H_p and H_u are the prediction and control horizons, respectively; Q and R are the weighting matrices, which are considered to be unchanged for the prediction horizon H_p.

The cost function (Equation (8)) can be represented as:

$$J(k) = \| Y(k) - T(k) \|_Q^2 + \| \Delta U \|_R^2 \tag{9}$$

where:

$$Y(k) = \begin{bmatrix} y(k|k) \\ \vdots \\ y(k+H_p-1|k) \end{bmatrix};\ T(k) = \begin{bmatrix} r(k|k) \\ \vdots \\ r(k+H_p-1|k) \end{bmatrix};\ \Delta U(k) = \begin{bmatrix} \Delta u(k|k) \\ \vdots \\ \Delta u(k+H_p-1|k) \end{bmatrix}$$

$$Q = \begin{bmatrix} Q & 0 & \dots & 0 \\ 0 & Q & \dots & 0 \\ \vdots & \vdots & \ddots & \vdots \\ 0 & 0 & \cdots & Q \end{bmatrix};\ R = \begin{bmatrix} R & 0 & \dots & 0 \\ 0 & R & \cdots & 0 \\ \vdots & \vdots & \ddots & \vdots \\ 0 & 0 & \cdots & R \end{bmatrix}$$

By deriving the prediction expressions (Equation (7)), we have:

$$Y(k) = \Psi x(k) + \Gamma u(k-1) + \Theta \Delta U(k) \tag{10}$$

where:

$$\Psi = \begin{bmatrix} C \\ CA \\ CA^2 \\ \vdots \\ CA^{H_p-1} \end{bmatrix};\ \Gamma = \begin{bmatrix} 0 \\ CB \\ CAB + CB \\ \vdots \\ C\sum_{i=0}^{H_p-2} A^i B \end{bmatrix};\ \Theta = \begin{bmatrix} 0 & 0 & \dots & 0 \\ CB & 0 & & \\ CAB + CB & & \ddots & \vdots \\ \vdots & & \ddots & 0 \\ C\sum_{i=0}^{H_u-2} A^i B & & \vdots & 0 \\ \vdots & & \ddots & \vdots \\ C\sum_{i=0}^{H_p-2} A^i B & & \vdots & C\sum_{i=0}^{H_p-H_u-1} A^i B \end{bmatrix}$$

It is also assumed that:

$$E(k) = \mathrm{T}(k) - \Psi x(k) - \Gamma u(k-1) \tag{11}$$

By substituting the prediction expression (Equation (10)) into the cost function (Equation (9)), the cost function can be represented as:

$$J(k) = \Delta U^T H' \Delta U - \Delta U^T G + E^T Q E \tag{12}$$

where:

$$G = 2\Theta^T Q E(k);\ H' = \Theta^T Q \Theta + R_j$$

The cost function (Equation (12)) can be minimized by quadratic programming (QP) to find the optimal values [18]. Since H' is positive due to the positive weighting matrices Q and R_j, the solution is given by:

$$\Delta U = \frac{1}{2} H'^{-1} G \tag{13}$$

When the solution of the cost function (Equation (12)) has been obtained, the output of the controller after optimization is given by Equation (14). Only the first value in the optimal trajectory, $u(k/k)$, is applied to the process. At the next sampling interval, the entire procedure is repeated.

$$u(k+i|k) = u(k+i-1/k) + \Delta u(k+i-1/k) \tag{14}$$

In this study, we consider the sampling time of MPC is equal to 0.01 s; the prediction horizon Hp is equal to 10; the control horizon is equal to 2; Q is equal to 0 and R_j is equal to 0.1.

3. Simulation Results

A comparison study of the MPC and PI regulator for secondary frequency control is presented in this section. In order to effectively compare these performances, PI parameters are tuned automatically by using the proportional–integral–derivative (PID) tuner provided by MATLAB/Simulink (Version 2015b, MathWorks, Natick, MA, USA). Several scenarios are carried out to evaluate the dynamic response and robustness of MPC-based secondary frequency control. Two types of WTGs, fixed-speed and variable-speed WTGs, are considered to show the impact of different WTG models on the control performance of MPC. The dynamic responses of both controllers are evaluated by examined the MG system under the conditions of load changing and wind power fluctuations. The robustness of the MPC-based secondary frequency control is analyzed by considering the system uncertainties.

3.1. Load Change and Wind Fluctuations

The frequency response of the MG system to the load changing is shown in Figure 4. The load connects to the MG system at 1 s with an amount of 0.02 pu, which results in the reduction of the frequency. The ESS with secondary frequency control generates more active power to recover the MG frequency to the nominal value. Figure 4b shows that the control performance of MG frequency regulation with MPC is much better than the PI regulator. The frequency response using MPC is faster and the overshoot is lower compared to the PI regulator.

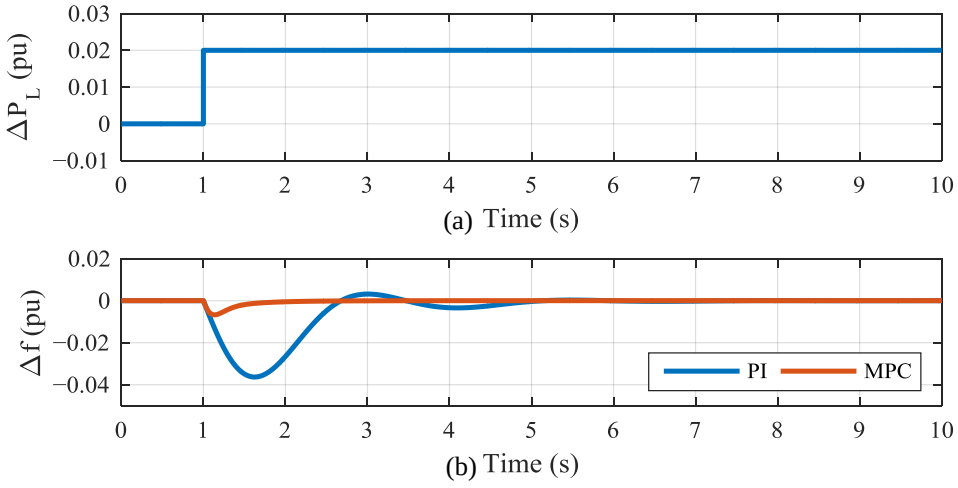

Figure 4. MG frequency when changing load: (**a**) load disturbance; and (**b**) frequency deviation.

Figure 5 shows the frequency response of the MG system under the condition of wind power fluctuation. The wind power increases from 0 pu to the average power of 0.03 pu. It can be seen that the frequency deviation of the MG system with the PI regulator is larger than that with MPC. A better performance of MPC is clearly observed from the frequency response of the MG system under the conditions of load change and wind power fluctuation.

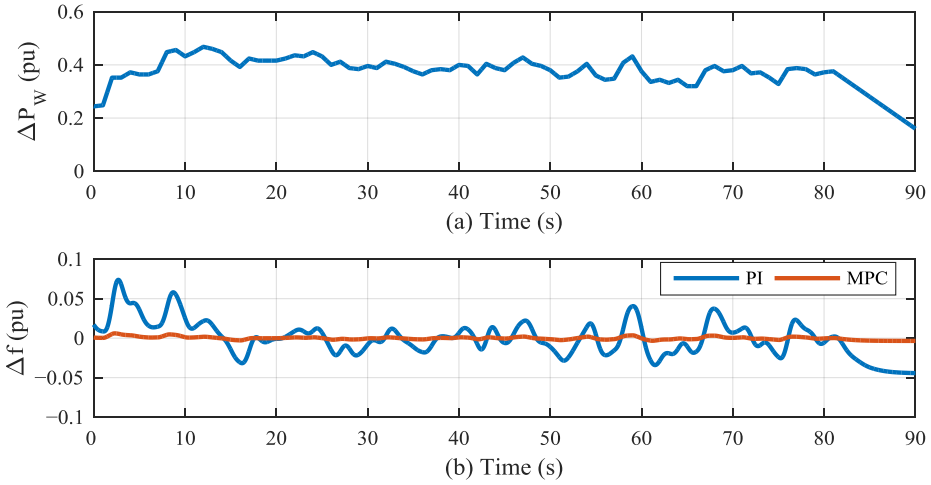

Figure 5. MG frequency when wind power fluctuates: (**a**) wind fluctuation; (**b**) frequency deviation.

3.2. Impacts of System Parameters on MPC

The operation of MPC is based on the model prediction that is used to estimate the future state variables. The control performance of MPC might be affected by the mismatch between the designed model parameters and the actual model parameters. In order to analyzed the impacts of the system parameters on the control performance of MPC, all parameters listed in Table 1 are varied significantly from −50% to +50%. Since the inertia time constant H is defined by the type and nominal power of the generator, the variation of the inertia time constant H can be neglected if the stand-alone MG has only one DG. However, the case where multiple DGs with different inertia time constants operate in parallel can exist in the stand-alone MG. In this case, the total inertia time constant of the DGs can be changed according to the operating configuration. Several studies have considered the variation of the inertia time constant H for designing the frequency controller in a MG [10,12,15,16,19]. Similar to previous works, only one DG is considered for the purpose of simplicity in this study. The variation of the inertia time constant H can be represented as different operating configurations of multiple DGs. A comparison study of MPC and PI control is presented in this section as well.

The trajectory of MG system poles with respect to the variation of the inertia time constant H is shown in Figure 6. It can be seen that the MG system with two controllers is sensitive to the variation of H. However, all poles of the MG system under either MPC or PI control are in the left-half plane (LHP), which demonstrates that the MG system is stable although the inertia time constant H varies significantly. However, the trajectory of poles λ_3 and λ_4 under MPC and PI control is different. In the case of the MG system with PI control, the two poles move towards the imaginary axis, which reduces the stability margin of the MG system. Meanwhile, in the case of the MG system with MPC, these poles move away from the imaginary axis, which increases the stability margin of the MG system. The frequency response of the MG system to the load change with an amount of 0.02 pu is shown in Figure 7. The overshoot of the MG frequency is reduced when H increases. It is observed that the frequency response of the MG system with PI control deviates significantly from the designed parameters (0% of H variation). By comparison, the performance of MPC-based frequency regulation varies slightly with the variation of H. MPC-based secondary frequency control achieves a better performance of the frequency response.

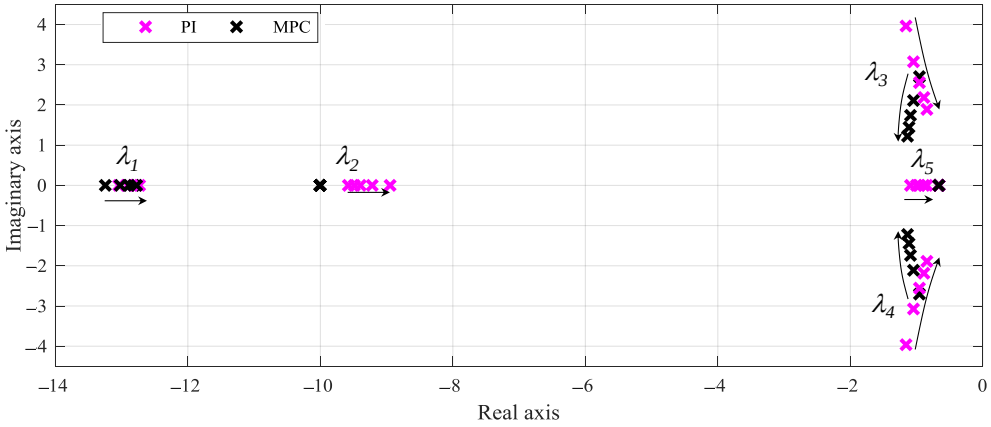

Figure 6. Trajectory of MG system poles when H varies from −50% to +50%.

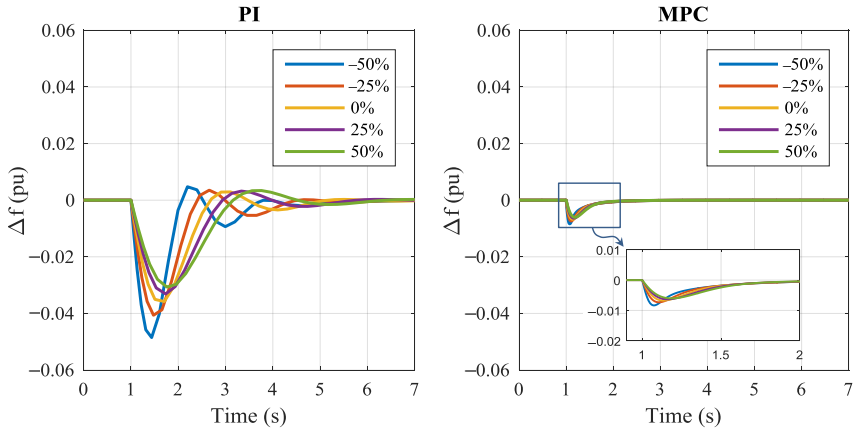

Figure 7. Frequency response to the load change when H varies from −50% to +50%.

The load damping D and governor time constant T_g have a slight impact on the frequency response of both controllers, as shown in Figures 8–11. All poles of the MG system using either MPC or the PI regulator are on the LHP, which shows that the MG system is stable with the variation of the load damping D and governor time constant T_g. The stability margin of the MG system decreases slightly when D and T_g increase. A better performance of frequency regulation and robustness against the variation of D and T_g can be achieved by MPC-based frequency control.

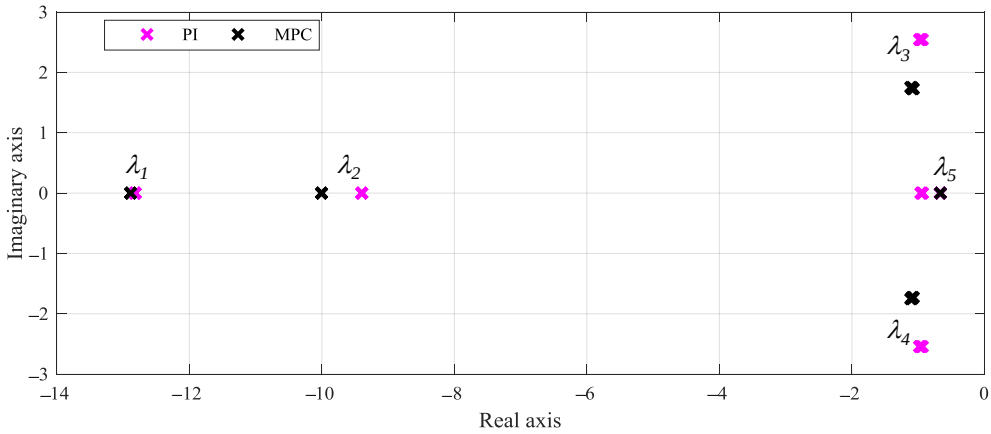

Figure 8. Trajectory of MG system poles when D varies from −50% to +50%.

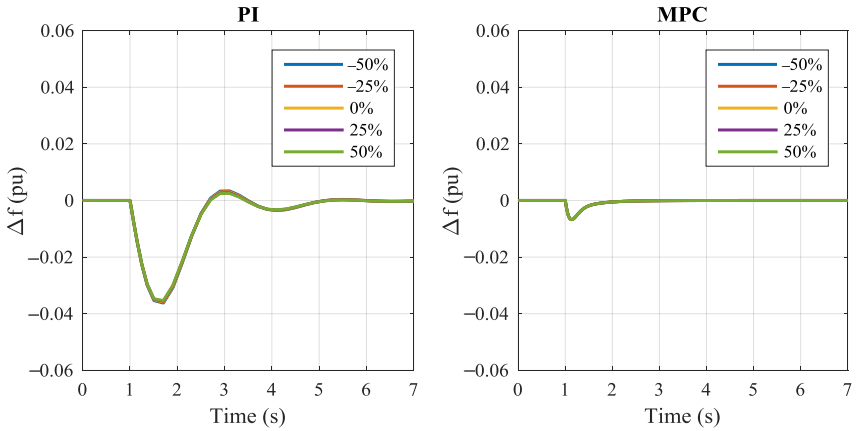

Figure 9. Frequency response to the load change when D varies from −50% to +50%.

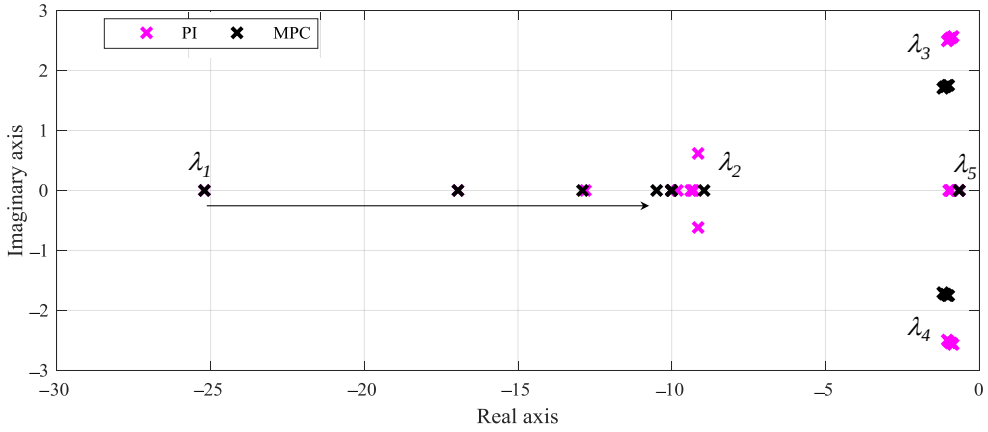

Figure 10. Trajectory of MG system poles when T_g varies from −50% to +50%.

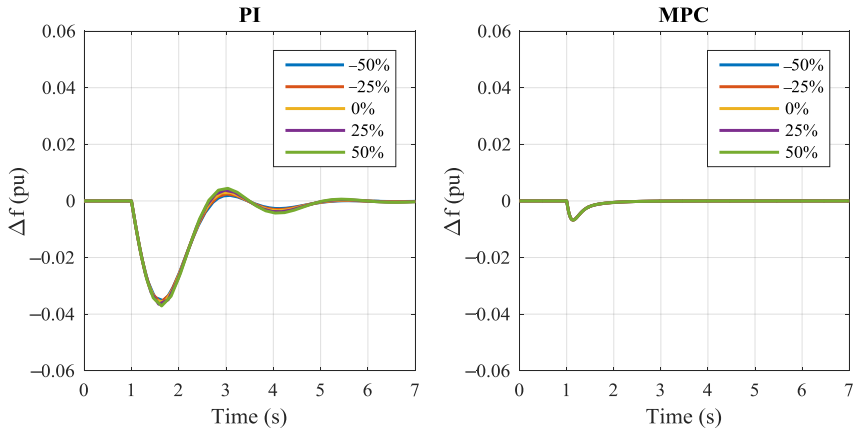

Figure 11. Frequency response to the load change when T_g varies from −50% to +50%.

Figure 12 shows the loci of the MG system poles when the turbine time constant T_t varies. All poles of the MG system using either MPC or the PI regulator located in the LHP demonstrate that the MG system is stable. However, the stability margin of the MG system is reduced when the time constant T_t increases due to the movement of the system poles towards the imaginary axis. Figure 13 shows the frequency response to the load change in this case. It can be seen that the MG system using PI control is sensitive to the variation of T_t. A better robustness against the variation of T_t is achieved by MPC.

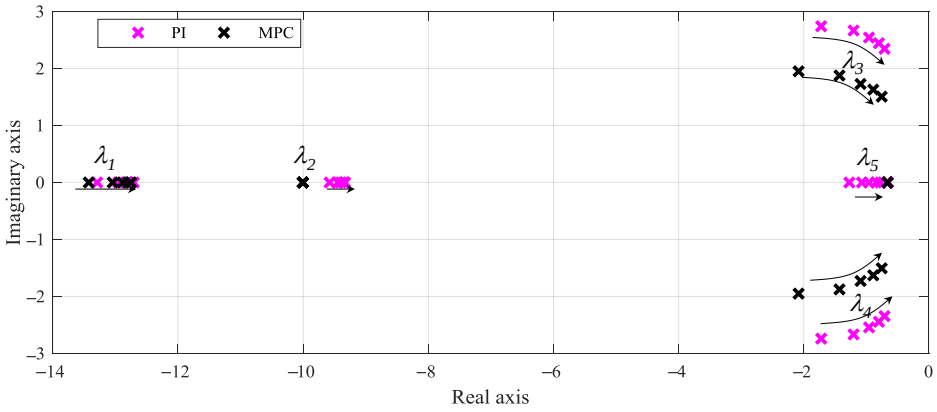

Figure 12. Trajectory of MG system poles when T_t varies from −50% to +50%.

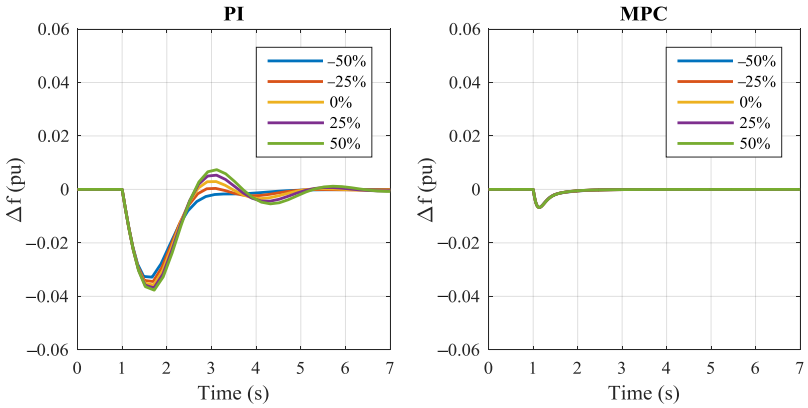

Figure 13. Frequency response to the load change when T_t varies from −50% to +50%.

The performance of the MG system using either MPC or PI control is analyzed with the variation of the droop constant R. The loci of the MG system poles shown in Figure 14 illustrates that the MG system using either MPC or PI control is still stable when R changes significantly. However, in the case of PI control, the poles λ_3 and λ_4 move towards the imaginary axis when R increases, which reduces the stability margin of the MG system. By comparison, in the case of MPC, the stability margin is slightly improved because these poles move away from the imaginary axis. The frequency response to the load change when R varies is shown in Figure 15. The MG system using PI control is sensitive to the variation of R, whereas the MG system using MPC is insensitive to the R variation.

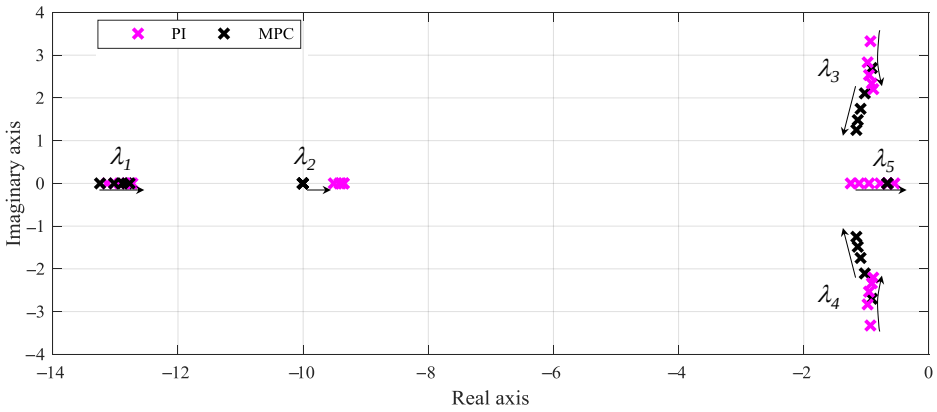

Figure 14. Trajectory of MG system poles when R varies from −50% to +50%.

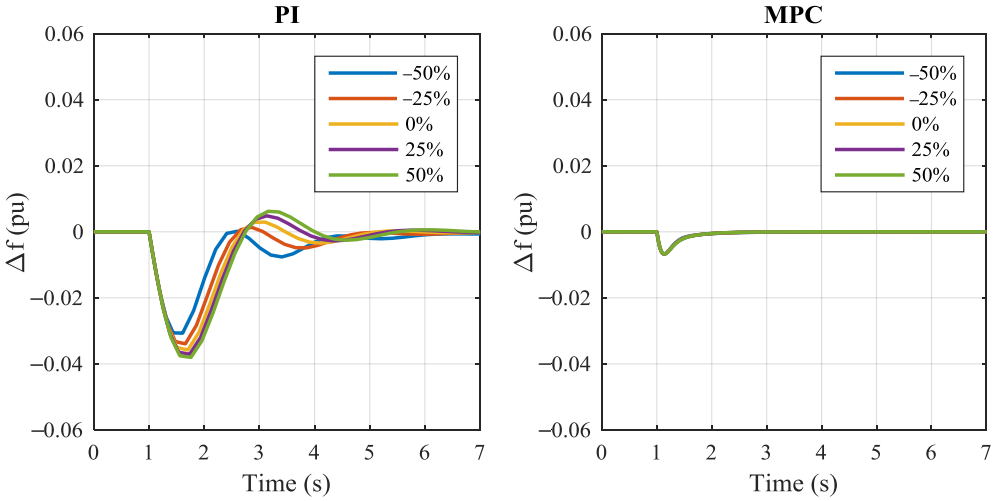

Figure 15. Frequency response to the load change when R varies from −50% to +50%.

Figure 16 shows the trajectory of the MG system poles when the ESS time constant T_E changes. The increase of T_E results in the reduction of system damping. The stability margin of the MG system using either MPC or PI control is reduced when T_E increases. However, the MG system using either MPC or PI control is still stable because all the poles of the MG system are in the LHP even though the ESS time constant T_E varies significantly. In the case of the MG system using MPC, the variation of T_E only has an impact on system damping. However, in the case of the MG system using PI control, the variation of T_E might cause an additional oscillation, which has an impact on the transient response performance. The frequency response to the load change is shown in Figure 17. It can be seen that the MG system using either MPC or PI control is slightly sensitive to the variation of T_E. In the case of the MG system using MPC, the increase of T_E leads to the slight reduction of response time and increase of overshoot. By comparison, in the case of the MG system with PI control, the increase of T_E results in the slight reduction of both the response time and overshoot. In general, MPC-based secondary frequency control still has better performance compared to the PI-based secondary frequency control.

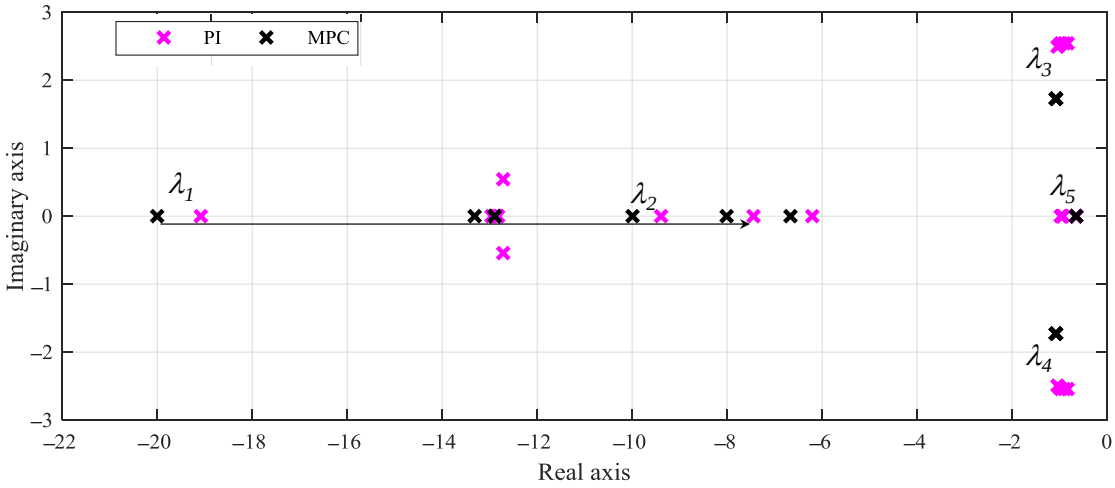

Figure 16. Trajectory of MG system poles when T_E varies from −50% to +50%.

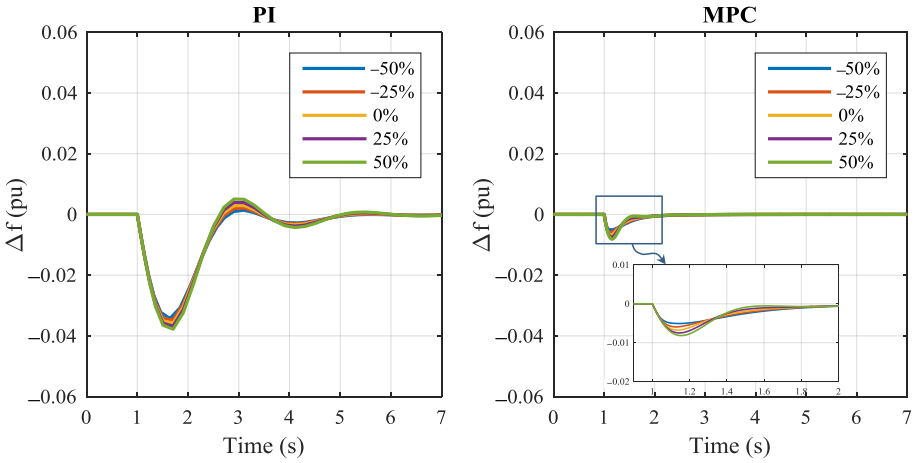

Figure 17. Frequency response to the load change when T_E varies from −50% to +50%.

The worst case corresponding to the variation of multiple system parameters that have a significant impact on the control performance is considered. In this case, the variation of the inertia time constant H is equal to −50%, the variation of turbine time constant T_t is equal to 50%, and the variation of the droop constant R is equal to −50%. The frequency response to the load change is shown in Figure 18. It can be seen that the control performance of the PI regulator is changed significantly. By comparison, there is a slight difference in the control performance of the MPC-based frequency regulation.

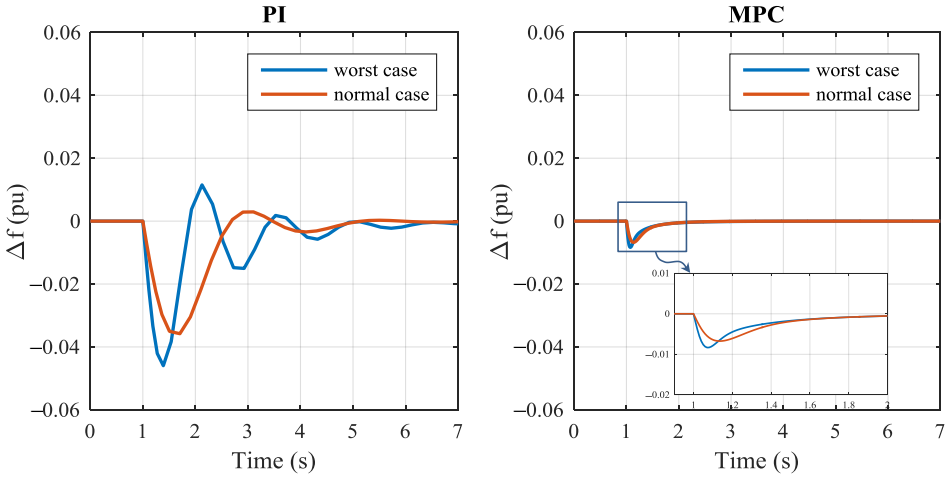

Figure 18. Frequency response in the worst case scenario.

3.3. Impacts of the Wind Generator Model on MPC

The use of variable-speed WTG based on a doubly fed induction generator (DFIG) has gained more attention recently due to the economic benefits. The impacts of WTG based on DFIG on the frequency control performance of MPC are evaluated in this section. Figure 19 shows the block diagram of such a WTG that includes the windmill and generator [19]. The following equations represent the characteristics of the windmill and generator.

$$P_{wo} = 0.5 C_p(\lambda, \beta) v_w^3 \rho A_w \tag{15}$$

$$C_p(\lambda, \beta) = c_1(\beta)\lambda^2 + c_2(\beta)\lambda^3 + c_3(\beta)\lambda^4 \tag{16}$$

$$\begin{cases} c_1(\beta) = c_{10} + c_{11}\beta + c_{12}\beta^2 + c_{13}\beta^3 + c_{14}\beta^4 \\ c_2(\beta) = c_{20} + c_{21}\beta + c_{22}\beta^2 + c_{23}\beta^3 + c_{24}\beta^4 \\ c_3(\beta) = c_{30} + c_{31}\beta + c_{32}\beta^2 + c_{33}\beta^3 + c_{34}\beta^4 \end{cases} \tag{17}$$

$$\lambda = \frac{R_w \omega}{v_w} \tag{18}$$

$$\omega = \int \frac{2}{J}(P_{wo} - P_w)dt \tag{19}$$

$$s = \frac{\omega_0 - \omega}{\omega_0} \tag{20}$$

$$P_w = \frac{-3V^2 s(1+s)R_2}{(R_2 - sR_1)^2 + s^2(X_1 + X_2)^2} \tag{21}$$

where c_{10}–c_{34} are the constants that represent the characteristics of the windmill. More details of this WTG can be found in [26].

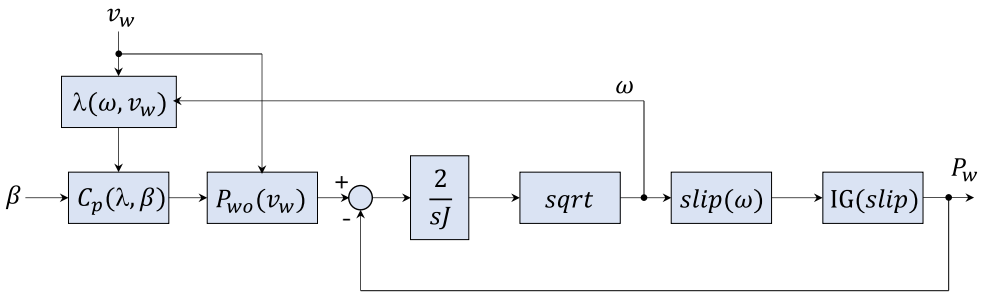

Figure 19. Configuration of the windmill and generator.

The wind power output can be regulated slightly by the change of the pitch angle β. Several studies have considered the change of the blade pitch angle for frequency regulation in a MG. This study mainly focuses on the controller of the ESS based on MPC, therefore, the pitch angle β can be assumed to be equal to zero. The parameters of the WTG are given in Table 2.

Table 2. Parameters of WTG, adopted from [26].

Windmill			**Generator**		
R_w	14 m	Rated power WTG	160 kW	R_2	0.00443 Ω
J	62,993 kg·m^2	V	380 V	X_1	0.0376 Ω
ρ	1.225 kg/m^3	R_1	0.00397 Ω	X_2	0.0534 Ω

The design process of MPC for ESS in this case is the same as in Section 2.2. The limitation power output of ESS is considered as ± 0.5625 pu. The output of the controller, $u(k/k)$, can be achieved by minimizing the cost function (Equation (8)) that is subjected to $-0.5625 \leq u(k) \leq 0.5625$.

Figure 20 shows the frequency response of the MG system when WTG based on DFIG is considered. Compared to Figure 5 where the fixed-speed WTG based on an induction generator is used, the frequency deviation of the MG using a variable-speed WTG is reduced slightly because the WTG based on DFIG has the ability to smoothen its power output. The complex model of the WTG has a slight impact on the control performance of MPC. However, the MPC-based frequency control still achieves better performance compared to the PI-based frequency control. For implementing MPC in a realistic MG system, the computation time of MPC should be considered, since the complexity of an overall MG system increases.

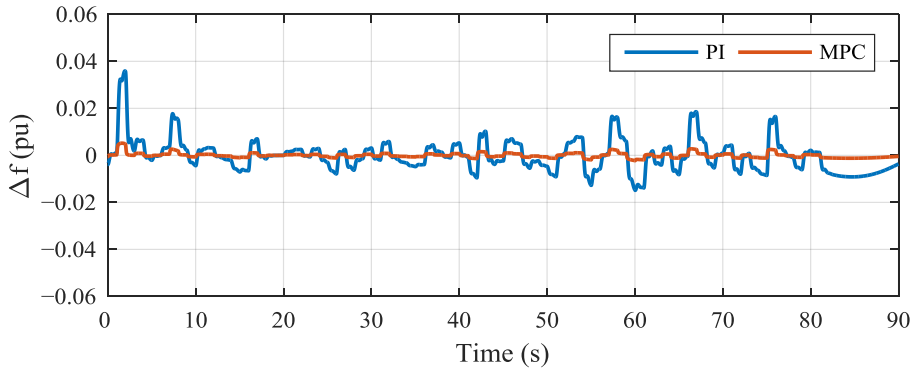

Figure 20. MG frequency deviation when a variable-speed WTG is used.

The robustness of MPC and the PI regulator against the significant variation of the turbine time constant T_t and the droop constant R is shown in Figure 21. It can be seen that the control performance of the PI regulator significantly deviates when the parameters change. By comparison, the control performance of the MPC strategy is stable for the variation of system parameters.

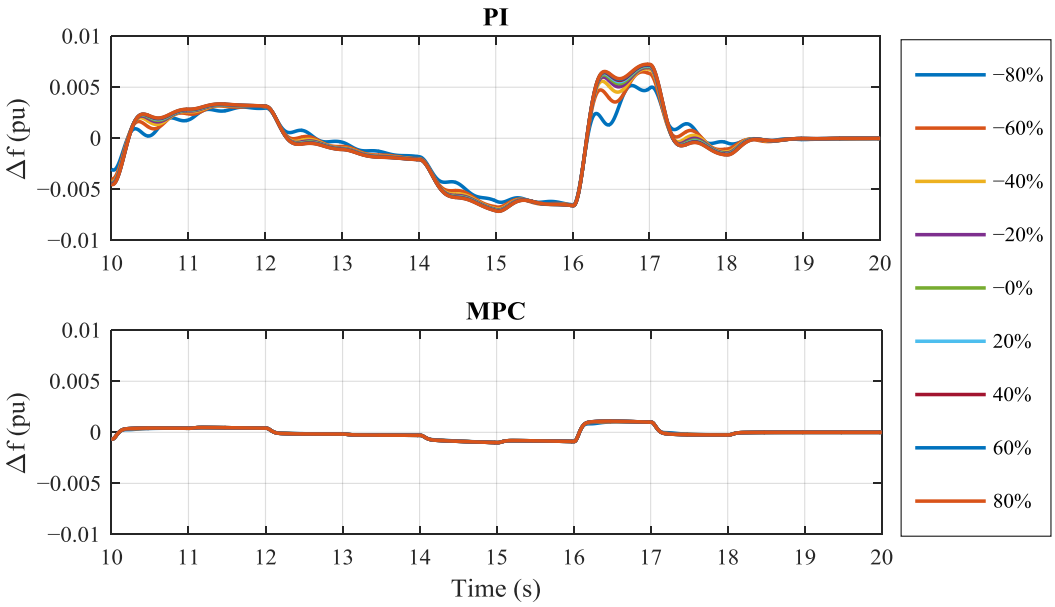

Figure 21. Frequency response when T_t and R vary from −80% to +80%.

4. Conclusions

The impacts of system parameters on the performance of MPC-based secondary frequency control have been analyzed in this study. The control performance of the MPC strategy was affected by the variations of the inertia time constant H and the ESS time constant T_E. The increase of H could reduce the overshoot while retaining the frequency response time. The increase of T_E could decrease the frequency response time, but the overshoot of the frequency response might increase.

A comparison study of MPC and PI based secondary frequency control for a stand-alone MG system has been also presented. Although the system parameters change significantly, the MG system using either MPC or PI control is still stable. The variations of the inertia time constant H, droop constant R, and turbine time constant T_t have a significant impact on the control performance of the PI regulator. However, these variations have a slight impact on the control performance of MPC. Simulation results showed that the robustness of MPC-based secondary frequency control against

the system uncertainties is stronger than that of PI control. The response time of MPC-based MG frequency regulation is faster than that of PI-based frequency control. For the MG system with a high penetration of wind generation, the MG frequency control based on PI control might exceed the allowable frequency deviation range. However, by using MPC-based secondary frequency control, the MG frequency could be maintained in the allowable frequency deviation range.

Both fixed-speed and variable-speed WTGs were considered to show the effect of the WTG model on the performance of the MPC strategy in a MG. The complex model of the variable-speed WTG might slightly affect the control performance of MPC. However, MPC-based frequency control still achieves better performance than the PI-based frequency control. The computation time of MPC should be considered due to the increasing complexity of the overall MG system.

The linearized stand-alone MG model used in this study is quite simplistic. For the application of MPC to a realistic MG system, testing MPC using the hardware-in-the-loop simulation will be considered in our future study.

Acknowledgments: This work was supported by the Incheon National University Research Grant in 2014.

Author Contributions: The paper was a collaborative effort between the authors. The authors contributed collectively to the theoretical analysis, modeling, simulation, and manuscript preparation.

Conflicts of Interest: The authors declare no conflict of interest.

Nomenclature

System parameters

H	Inertial time constant of diesel generator
D	Load damping
R	Droop constant
T_t	Turbine time constant
T_g	Governor time constant
T_E	ESS time constant
T_W	Time constant of wind generator
ΔP_L	Load deviation
ΔP_m	The change of mechanical power
ΔP_E	The change of ESS power
ΔP_W	The change of wind power
Δw	The change of wind speed
ΔP_g	The change of governor output
ΔP_c	The change of primary control output
Δf	Frequency deviation

Parameters of WTG based on DFIG

A_w	Cross section of rotor for windmill
C_p	Power coefficient of windmill
λ	Tip speed ratio
ρ	Air density
J	Moment of inertia for windmill
v_w	Wind speed
P_w	Wind power output
P_{wo}	Windmill power output
R_w	Radius of windmill
ω_0	Synchronous angular speed
ω	Angular rotor speed
V	Phase voltage of generator
X_1, X_2	Reactance of stator and rotor, respectively
R_1, R_2	Resistance of stator and rotor, respectively

References

1. Olivares, D.E.; Mehrizi-Sani, A.; Etemadi, A.H.; Canizares, C.A.; Iravani, R.; Kazerani, M.; Hajimiragha, A.H.; Gomis-Bellmunt, O.; Saeedifard, M.; Palma-Behnke, R.; et al. Trends in Microgrid Control. *IEEE Trans. Smart Grid* **2014**, *5*, 1905–1919. [CrossRef]
2. Gu, W.; Liu, W.; Wu, Z.; Zhao, B.; Chen, W. Cooperative Control to Enhance the Frequency Stability of Islanded Microgrids with DFIG-SMES. *Energies* **2013**, *6*, 3951–3971. [CrossRef]
3. Unamuno, E.; Barrena, J.A. Equivalence of Primary Control Strategies for AC and DC Microgrids. *Energies* **2017**, *10*, 91. [CrossRef]
4. Kim, Y.-S.; Kim, E.-S.; Moon, S.-I. Frequency and Voltage Control Strategy of Standalone Microgrids with High Penetration of Intermittent Renewable Generation Systems. *IEEE Trans. Power Syst.* **2016**, *31*, 718–728. [CrossRef]
5. Kim, Y.-S.; Hwang, C.-S.; Kim, E.-S.; Cho, C. State of Charge-Based Active Power Sharing Method in a Standalone Microgrid with High Penetration Level of Renewable Energy Sources. *Energies* **2016**, *9*, 480. [CrossRef]
6. Jang, Y.-S.; Park, J.; Yoon, Y.T. Designing Structure-Dependent MPC-Based AGC Schemes Considering Network Topology. *Energies* **2015**, *8*, 3437–3454. [CrossRef]
7. Vandoorn, T.L.; Vasquez, J.C.; Kooning, J.D.; Guerrero, J.M.; Vandevelde, L. Microgrids: Hierarchical Control and an Overview of the Control and Reserve Management Strategies. *IEEE Ind. Electron. Mag.* **2013**, *7*, 42–55. [CrossRef]
8. Yang, J.-S.; Choi, J.-Y.; An, G.-H.; Choi, Y.-J.; Kim, M.-H.; Won, D.-J. Optimal Scheduling and Real-Time State-of-Charge Management of Energy Storage System for Frequency Regulation. *Energies* **2016**, *9*, 1010. [CrossRef]
9. Lotfy, M.E.; Senjyu, T.; Farahat, M.A.-F.; Abdel-Gawad, A.F.; Yona, A. A Frequency Control Approach for Hybrid Power System Using Multi-Objective Optimization. *Energies* **2017**, *10*, 80. [CrossRef]
10. Bevrani, H.; Habibi, F.; Babahajyani, P.; Watanabe, M.; Mitani, Y. Intelligent Frequency Control in an AC microgrid: Online PSO-based fuzzy tuning approach. *IEEE Trans. Smart Grid* **2012**, *3*, 1935–1944. [CrossRef]
11. Kim, J.-Y.; Kim, H.-M.; Kim, S.-K.; Jeon, J.-H.; Choi, H.-K. Designing an Energy Storage System Fuzzy PID Controller for Microgrid Islanded Operation. *Energies* **2011**, *4*, 1443–1460. [CrossRef]
12. Bevrani, H.; Feizi, M.R.; Ataee, S. Robust Frequency Control in an Islanded Microgrid: H_∞ and μ -Synthesis Approaches. *IEEE Trans. Smart Grid* **2016**, *7*, 706–717.
13. Su, X.; Han, M.; Guerrero, J.M.; Sun, H. Microgrid Stability Controller Based on Adaptive Robust Total SMC. *Energies* **2015**, *8*, 1784–1801. [CrossRef]
14. Vachirasricirikul, S.; Ngamroo, I. Robust LFC in a Smart Grid with Wind Power Penetration by Coordinated V2G Control and Frequency Controller. *IEEE Trans. Smart Grid* **2014**, *5*, 371–380. [CrossRef]
15. Han, Y.; Young, P.M.; Jain, A.; Zimmerle, D. Robust Control for Microgrid Frequency Deviation Reduction with Attached Storage System. *IEEE Trans. Smart Grid* **2015**, *6*, 557–565. [CrossRef]
16. Hossain, M.J.; Pota, H.R.; Mahmud, M.A.; Aldeen, M. Robust Control for Power Sharing in Microgrids with Low-Inertia Wind and PV Generators. *IEEE Trans. Sustain. Energy* **2014**, *6*, 1067–1077. [CrossRef]
17. Lewis, F.L.; Dawson, D.M.; Abdallah, C.T. *Robot Manipulator Control: Theory and Practice*; Marcel Dekker Inc.: New York, NY, USA, 2004.
18. Wang, L. *Model Predictive Control System Design and Implementation Using MATLAB®*; Springer: London, UK, 2009.
19. Pahasa, J.; Ngamroo, I. Coordinated Control of Wind Turbine Blade Pitch Angle and PHEVs Using MPCs for Load Frequency Control of Microgrid. *IEEE Syst. J.* **2016**, *10*, 97–105. [CrossRef]
20. Pahasa, J.; Ngamroo, I. PHEVs Bidirectional Charging/Discharging and SoC Control for Microgrid Frequency Stabilization Using Multiple MPC. *IEEE Trans. Sustain. Energy* **2015**, *6*, 526–533. [CrossRef]
21. Yang, J.; Zeng, Z.; Tang, Y.; Yan, J.; He, H.; Wu, Y. Load Frequency Control in Isolated Micro-Grids with Electrical Vehicles Based on Multivariable Generalized Predictive Theory. *Energies* **2015**, *8*, 2145–2164. [CrossRef]
22. Wen, G.; Hu, G.; Hu, J.; Shi, X.; Chen, G. Frequency Regulation of Source-Grid-Load Systems: A Compound Control Strategy. *IEEE Trans. Ind. Inform.* **2016**, *12*, 69–78.

23. Nguyen, T.-T.; Yoo, H.-J.; Kim, H.-M. Application of Model Predictive Control to BESS for Microgrid Control. *Energies* **2015**, *8*, 8798–8813. [CrossRef]
24. Bevrani, H. *Robust Power System Frequency Control*, 2nd ed.; Springer: Gewerbestrasse, Switzerland, 2014.
25. Liu, X.; Zhang, Y.; Lee, K.Y. Coordinated Distributed MPC for Load Frequency Control of Power System with Wind Farms. *IEEE Trans. Ind. Electron.* **2016**. [CrossRef]
26. Senjyu, T.; Sakamoto, R.; Urasaki, N.; Funabashi, T.; Fujita, H.; Sekine, H. Output Power Leveling of Wind Turbine Generators Using Pitch Angle Control for All Operating Regions in Wind Farm. *IEEE Trans. Energy Convers.* **2006**, *21*, 467–475. [CrossRef]